Modulation of Electronic Structure of Armchair MoS2 Nanoribbon

ARTICLE *in* THE JOURNAL OF PHYSICAL CHEMISTRY C · SEPTEMBER 2015

Impact Factor: 4.77 · DOI: 10.1021/acs.jpca.5b04747 · Source: PubMed

THE JOURNAL OF PHYSICAL CHEMISTRY C

Article

pubs.acs.org/JPCC

Modulation of Electronic Structure of Armchair MoS_2 Nanoribbon

Long Zhang,[†] Langhui Wan,[*,†] Yunjin Yu,[†] Bin Wang,[†] Fuming Xu,[†] Yadong Wei,[*,†] and Yang Zhao[‡]

[†]College of Physics Science and Technology, and Institute of Computational Condensed Matter Physics, Shenzhen University, Shenzhen 518060, People's Republic of China

[‡]School of Materials Science and Engineering, Nanyang Technological University, Singapore 639798

ABSTRACT: We perform first-principles calculations on electronic structures of armchair MoS_2 nanoribbons ($AMoS_2NRs$) passivated by non-metal atoms. In contrast to bare $AMoS_2NR$ ($AMoS_2NR$-bare) or purely hydrogen (H) edge-terminated $AMoS_2NR$ ($AMoS_2NR$-H), it is found that H and oxygen (O) hybrid edge-terminated $AMoS_2NR$ ($AMoS_2NR$-H-O) is more stable. $AMoS_2NR$-H-O exhibits a direct band gap of about 1.43 eV, which is larger than those of pristine $AMoS_2NR$ (about 0.61 eV) and $AMoS_2NR$-H (about 0.60 eV) and even exceeds the band gap of bulk MoS_2 (about 0.86 eV) and is close to that of monolayer MoS_2 (about 1.67 eV). The remarkable band gap of $AMoS_2NR$-H-O is attributed to the charge redistribution on the edge atoms of the MoS_2 nanoribbon, especially the charges on the edge Mo atoms. Detailed calculations of $AMoS_2NR$-H-O reveal that over 70% of the total density of states (DOS) of the conduction band minimum and the valence band maximum are contributed by the Mo atoms. In particular, edge Mo atoms play a crucial role in modulating the electronic structure. In addition, we have studied a series of functionalized $AMoS_2NR$-H-X with X = S, F, C, N, and P, respectively. It is found that $AMoS_2NR$-H-X with X = S, 2F, C possess remarkable electronic band gaps, whereas $AMoS_2NR$-H-X with X = F, N, P are metallic. Our studies suggest that non-metal atom hybrid passivation can efficiently tune the electronic band gap of MoS_2 nanoribbon and open a new route to obtain a MoS_2-based practical nanoelectronic device and a photovoltaic device.

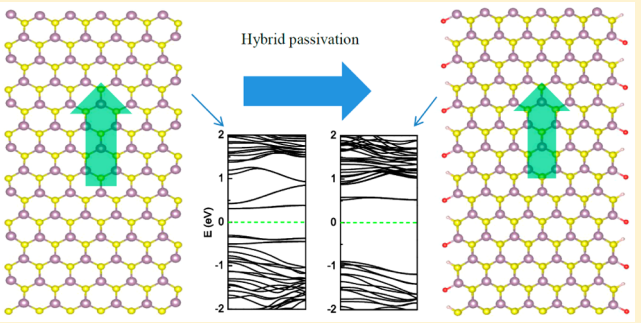

I. INTRODUCTION

Over the past decade, two-dimensional (2D) materials are increasingly found in nanoelectronic and new photonic devices due to their remarkable electronic properties.[1] In particular, graphene has attracted great interest because of its unique properties. Pristine graphene exhibits metallic behavior with no band gap, whereas modified graphene can have finite band gaps. As the band gap is critical to devices such as logic transistors or solar cells,[2] several approaches on graphene band gap engineering have been presented, such as graphene nanoribbon synthesis,[3] bilayer control,[4,5] and chemically modified graphene.[6−9] However, most of these efforts have failed to achieve a large band gap.[10] Besides, some of the methods are subject to mobility trade−off or less stability.[11]

To date, many authors focus their attention on the practical properties of monolayer MoS_2, one of the monolayer transition metal disulfide (TMD).[12−15] Monolayer MoS_2 is a 2D promising material as a potential complement to graphene and has been found to be an excellent candidate for field effect transistors (FET) with on/off ratio exceeding 10^8 (see ref 16) and valley-based electronic devices.[17] Recent reports on FET devices composed of a MoS_2−graphene heterostructure are also given to combine the advantage of high carrier mobility in graphene with the permanent band gap of MoS_2 for digital applications.[18] It is obvious that band gap engineering of MoS_2 is quite important. Earlier work shows that bulk MoS_2 possesses an indirect band gap of 1.2 eV and the monolayer MoS_2 presents a direct band gap of 1.8 eV.[19,20] A stable monolayer MoS_2 owns a sandwiched structure where the Mo atom layer is sandwiched by two S atom layers (S−Mo−S structure) through strong covalent bonds in prismatic coordination. For bulk MoS_2, the neighboring monolayer is stacked one by one through the weak van der Waals force.[21] Considerable efforts have been devoted to synthesize the MoS_2 monolayer, including a variety of exfoliations,[22,23] physical vapor deposition (PVD),[24] and chemical vapor deposition (CVD).[25] Very recently, Lee et al.[26] demonstrated the growth of high-quality MoS_2 monolayer using ambient-pressure chemical vapor deposition.

More recently, MoS_2 one-dimensional (1D) nanostructures, such as nanoribbons, nanotubes, wires, and rods, have drawn considerable attention to understand their intrinsic properties.[27] Lots of works try to study the wide array of the electronic transport properties, photovoltaic systems, and photodetectors, etc.[28] From a nanostructure perspective, 1D structures show a range of potential applications which are quite different from those presented by their 2D and 3D counterparts.[29,30] MoS_2 nanoribbons and other TMD nanoribbons have been synthesized by chemical unzipping of nanotubes[31] or the top-down approach (MoS_2 sheet under electron irradiation).[32] Although a remarkable reduction in carrier mobility occurs for graphene in

Received: May 19, 2015
Revised: August 1, 2015

DOI: 10.1021/acs.jpcc.5b04747
J. Phys. Chem. C XXXX, XXX, XXX−XXX

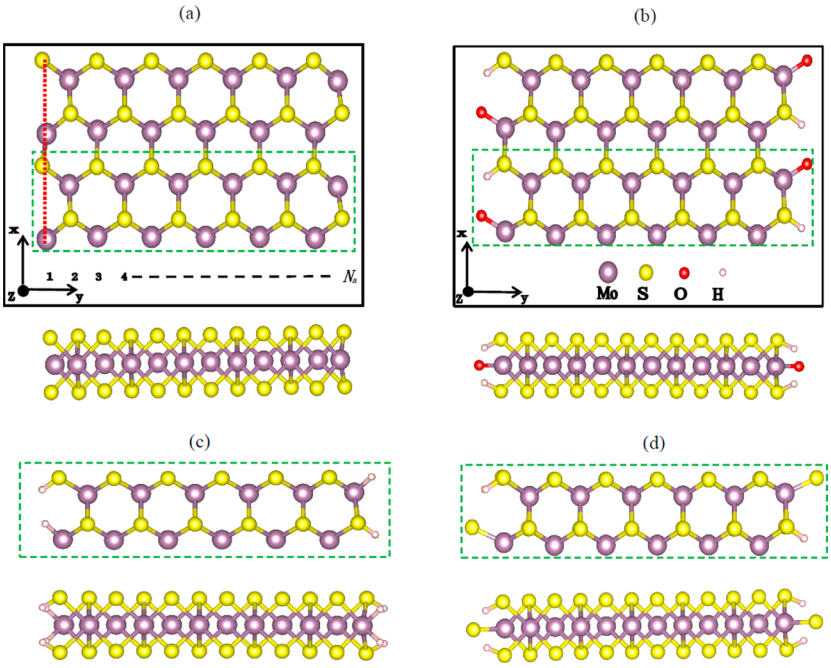

Figure 1. Top and side views of the armchair MoS_2 nanoribbons with $N_a = 12$ for (a) bare ribbon ($A12MoS_2NR$-bare), (b) H- and O-terminated ribbon ($A12MoS_2NR$-H-O), (c) H-terminated ribbon ($A12MoS_2NR$-H), and (d) H- and S-terminated ribbon ($A12MoS_2NR$-H-S).

its nanoribbon form, robust carrier mobility is found in monolayer MoS_2 nanoribbon.[33] This feature makes the MoS_2 nanoribbon an ideal 1D material of nanoelectronic devices. Furthermore, electronic structures of nanoribbons can be modified by manipulating its edges,[34,35] offering a powerful tool for customizing such nanostructure to particular applications.[36−38] In contrast to the 2D and 3D counterparts, the band structure of the MoS_2 nanoribbon is more complex.[39−41] For instance, zigzag MoS_2 nanoribbons are a magnetic metal and exhibit ferromagnetic edge states, but armchair MoS_2 nanoribbons ($AMoS_2NR$) behave as a nonmagnetic semiconductor. As the nanoribbon width increases, the band gap of $AMoS_2NR$ converges to 0.56 eV.[42]

To engineer the band structure, edge modification is certainly a promising option. The most commonly used edge passivation is hydrogenation. The rate of edge hydrogenation is determined by temperature, pressure, and concentration of H_2 in the passivation process. The controllable process of passivation can make various edge hydrogenations of $AMoS_2NR$, such as terminating each edge S atom by one H atom and each edge Mo atom by one H atom or without an H atom, or terminating each edge Mo atom by two H atoms and an S atom without an H atom.[43,44] By using density functional theory (DFT), Sagynbaeva et al.[45] explore electronic structures and magnetic properties of the MoS_2 nanoribbon with hydrogen passivation or carbon passivation. However, such chemical functionalization may not be stable because of the relatively weak S−H and Mo−H bonds.[46] Moreover, according to our calculations, the band gaps of hydrogen saturated $AMoS_2NR$ and other single-atom edge passivation $AMoS_2NR$ still remain much smaller than those of bulk MoS_2 and monolayer MoS_2. A couple of questions arise promptly: can we find another passivation pattern to tune the band gap of MoS_2 nanoribbon? How does such edge chemical functionalization affect the electronic properties and stability of MoS_2 nanoribbons? The answers to these questions are quite important for the applications of 1D nanomaterial, and it is the point of our paper.

In this paper, by using density functional theory (DFT), we report a first-principles calculation of band gap modulation in $AMoS_2NRs$ by passivating the ribbon edges with non-metal atoms. In contrast to pristine MoS_2 nanoribbon and hydrogen-passivated $AMoS_2NRs$, we find that the MoS_2 nanoribbons are more stable when each edge Mo atom is terminated by one O atom and each edge S atom is terminated by one H atom. More interestingly, due to this new edge functionalization, the band gap of MoS_2 ribbon dramatically increases and exhibits a direct band gap of about 1.43 eV. Analysis of the electronic band structures shows that this remarkable band gap is attributed to the new bonds between the edge Mo and external O atoms. Our studies reveal the new possibility of tuning the band gap of MoS_2 nanoribbon and open up new routes for developing novel nanoelectronic devices and photovoltaic devices.

II. COMPUTATIONAL DETAILS

In Figure 1, several armchair MoS_2 nanoribbons with or without edge-terminated atoms are shown. In each panel from Figure 1a−d, a dashed-line (green) box encases one unit cell of the MoS_2 nanoribbon. x denotes the ribbon direction, and y, the width direction. According to the conventional notation, the width parameter N_a is defined as the number of armchair lines (see the vertical red dotted line in Figure 1a) across the ribbon width. In this work, we set $8 \leq N_a \leq 20$ and use the 1D periodic boundary condition (PBC) along the x direction. For structural optimization, we perform density functional theory (DFT) calculations by using the projector augmented wave (PAW) method as implemented in the Vienna *ab initio* simulation package (VASP).[47,48] The exchange and correlation potential is the Perdew−Burke−Ernzerhof functional (PBE)[49] and is treated using the generalized gradient approximation (GGA).[50] We set a kinetic energy cut off of 360 eV. The vacuum space is set to be 20 Å to avoid the interactions between nanoribbon and its periodic images. A k-point sampling of $10 \times 1 \times 1$ is used in relaxation. All ribbon structures are fully relaxed without considering spin

DOI: 10.1021/acs.jpcc.5b04747
J. Phys. Chem. C XXXX, XXX, XXX−XXX

polarization. The energy convergence threshold is 0.01 meV and the Hellmann−Feynman force is less than 0.01 eV/Å.

After structural relaxation, the band structures and the density of states are calculated using the Nanodcal software,[51,52] which is based on a combination of DFT and the nonequilibrium Green's function approach. A denser mesh of 200 × 1 × 1 is used to calculate binding energies, density of states (DOS), and band structures.

III. RESULTS AND DISCUSSION

a. 2D MoS_2 Monolayer and 1D Monolayer Armchair MoS_2 Nanoribbons. Before addressing the non-metal atom edge-terminated nanoribbons, we calculate the electronic band structures of single-layer MoS_2 and bare-edge single-layer armchair MoS_2 nanoribbons for benchmarking. Before structural relaxation, we set a lattice constant of 3.17 Å, a Mo−S bond length of 2.41 Å, a Mo−S−Mo (or S−Mo−S) bond angle of 82.36°, and a single-layer MoS_2 thickness of 3.13 Å. First, we calculate the band structure of the single-layer MoS_2, which is found to be semiconducting with a direct band gap of 1.67 eV in good agreement with previous studies.[42,53] Then, we make a full relaxation for the bare armchair MoS_2 nanoribbons ($AMoS_2$NR-bare) with a width ranging from N_a = 8 to N_a = 20. A full relaxation sees slight changes in structural parameters of the two edges (Table 1). We then calculate the binding energies and the band structures. As the nanoribbon width increases, the band gap converges to around 0.63 eV (Figure 2a), a value slightly larger than the previous computed band gap of about 0.07 eV.[33,42] Figure 2b shows that the band gap of $AMoS_2$NR-H-O is close to 1.43 eV, which is much larger than the band gap of $AMoS_2$NR-bare.

Table 1. Bond Distances (Å), Bond Angles θ (deg) at the Edge of Nanoribbons, Binding Energies E_b (eV), and Band Gaps E_g (eV) of Different A12MoS_2NRs

	structural parameters						
edge type	d_{Mo-X}	d_{S-H}	d_{S-Mo}	d_{S-S}	θ	E_b	E_g
NR-bare			2.29	3.20	82.61		0.61
NR-H	1.70	1.36	2.34	3.27	81.79	−2.54	0.60
NR-H-O	1.73	1.36	2.55	3.22	82.12	−5.81	1.41
NR-H-S	2.14	1.36	2.53	3.20	80.91	−3.55	1.09
NR-H-F	1.92	1.36	2.53	3.22	84.23	−3.45	0
NR-H-2F	1.94	1.37	2.50	3.13	81.63	−3.03	0.99
NR-H-C	1.83	1.38	2.48	3.25	79.80	−4.10	0.94
NR-H-N	1.70	1.37	2.55	3.20	82.78	−3.57	0
NR-H-P	2.17	1.40	2.55	3.27	81.07	−3.01	0

b. Hydrogenated Armchair MoS_2 Nanoribbons. Edge termination by hydrogenation is the simplest way to passivate the nanoribbon. But different edge hydrogenation patterns lead to different electronic properties. Here, we repeat the calculation on the fully hydrogen passivated A12MoS_2NR (A12MoS_2NR-H) for stability comparisons with other hybrid passivations. For H and X (X = O, S, F, C, N, P) hybrid-terminated A12MoS_2NR (A12MoS_2NR-H-X), we define the binding energy per atom $E_{\text{binding energy}}$ as

$$E_{\text{binding energy}} = (E_{H-X} - E_{\text{bare}} - mE_H - nE_X)/(n + m)$$

where E_{bare} and E_{H-X} are the total energies of nanoribbon in one unit cell with bare edges and with both H- and X-terminated edges, respectively. E_H and E_X are the energies of the isolated H atom and isolated X atom, respectively. m is the number of H atoms in one unit cell and n is the number of X atoms in one unit cell. For example, in our A12MoS_2NR-H configuration, each edge S atom is terminated by one H atom and each edge Mo atom is terminated by two H atoms, so there are eight hydrogen atoms in one unit cell (but zero X atom). In this case, we set m = 8, n = 0. The negative binding energy for A12MoS_2NR-H is −2.54 eV (Table 1), which indicates that one can stabilize the armchair MoS_2 nanoribbon by passivating the dangling bonds at edges with H atoms.

In Figure 3, we show the energy band diagrams of several armchair MoS_2 nanoribbons with N_a = 12 in the absence of spin polarization.[54] Panels a and b of Figure 3 are for pristine A12MoS_2NR and A12MoS_2NR-H. Panels c and d of Figure 3 are for hybrid passivation ribbons of A12MoS_2NR-H-O and A12MoS_2NR-H-S.

Comparing the band structures of A12MoS_2NR-bare and A12MoS_2NR-H (Figure 3a,b, respectively), one finds that the band gap of A12MoS_2NR-bare is 0.61 eV, and that of A12MoS_2NR-H, 0.60 eV. For more detailed analysis, we plot the projected density of states (PDOS) in Figure 4a,b for A12MoS_2NR-bare and A12MoS_2NR-H, respectively. It is found that frontier orbitals originate mainly from d orbitals of Mo atoms and partly from p orbitals of S atoms for both structures.

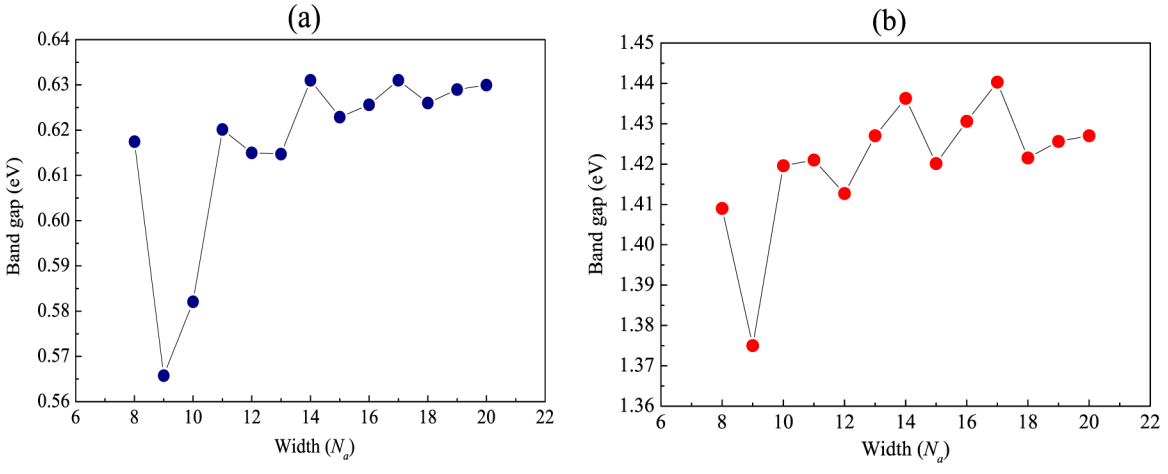

Figure 2. Energy band gap as a function of the ribbon width N_a with 8 ≤ N_a ≤ 20 for (a) $AMoS_2$NR-bare and (b) $AMoS_2$NR-H-O.

DOI: 10.1021/acs.jpcc.5b04747
J. Phys. Chem. C XXXX, XXX, XXX−XXX

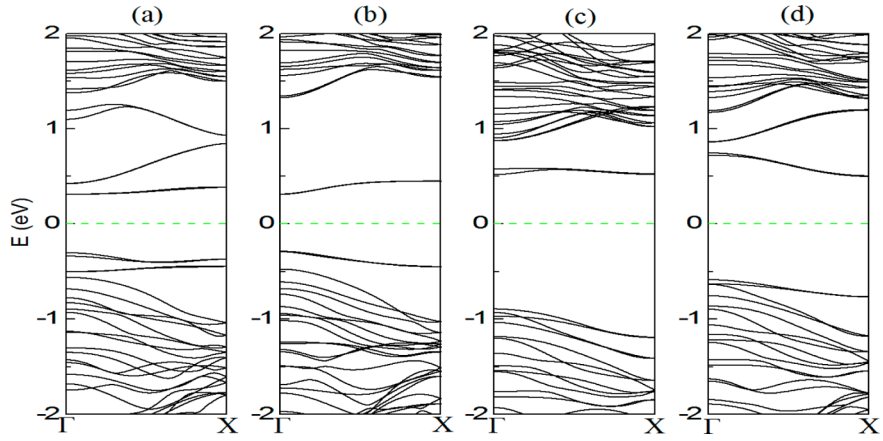

Figure 3. Energy band structures for (a) A12MoS_2NR-bare, (b) A12MoS_2NR-H, (c) A12MoS_2NR-H-O, and (d) A12MoS_2NR−H-S.

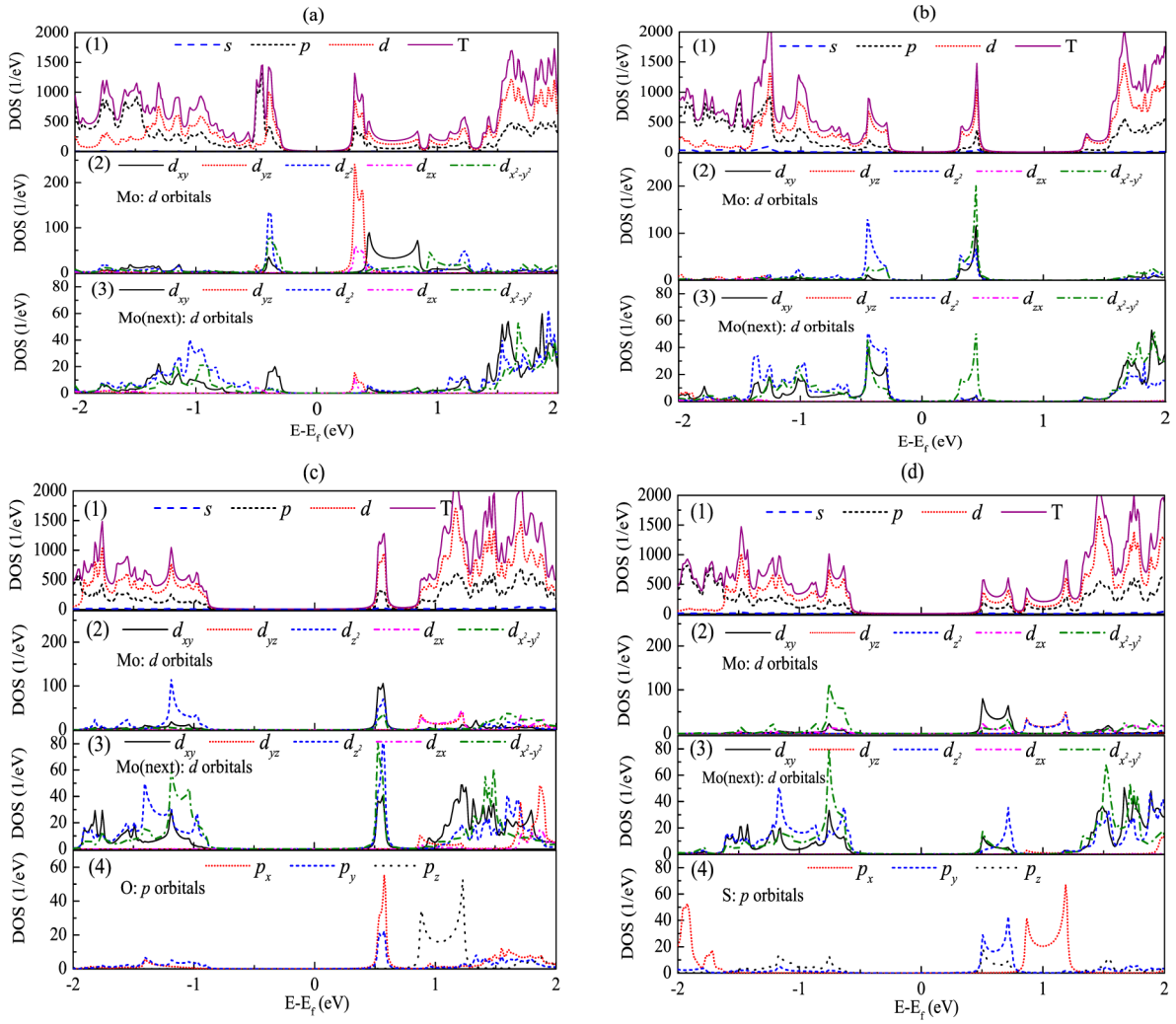

Figure 4. Total density of states (DOS) and projected density of states (PDOS) of different A12MoS_2NRs. (a) A12MoS_2NR-bare: (1) total DOS and DOS projected on orbitals. Notations are s for s orbital DOS, p for p orbital DOS, d for d orbital DOS, and T for total DOS. (2) PDOS of d orbitals on the very edge Mo atoms. (3) PDOS of d orbitals on the next edge Mo atoms. (b) A12MoS_2NR-H: the symbols are the same as in (a). (c) A12MoS_2NR-H-O: from (1) to (3), the symbols are same as in (a), and (4) is for PDOS of p orbitals of O atoms. (d) A12MoS_2NR-H-S: from (1) to (3), the symbols are same as in (a), and (4) is for PDOS of p orbitals of external S atoms.

The two ribbons have different compositions in the conduction band minimum (CBM) and the valence band maximum (VBM).

It is also found that the edge Mo atom plays a very important role in the CBM. For example, d_{yz} and d_{zx} orbitals of the edge Mo atom have strong influences (about 45% of total DOS) over the CBM of A12MoS_2NR-bare. The Mo atom next to the edge Mo atom contributes 4% of the total DOS with the rest contributed by the remaining Mo atoms (18% of total DOS) and the S atoms

DOI: 10.1021/acs.jpcc.5b04747
J. Phys. Chem. C XXXX, XXX, XXX−XXX

Table 2. Charges (e) on the Edge Atoms of Different A12MoS$_2$NRs

structure	Mo (edge)	S (edge)	H(−S)	H(−Mo)	O	S	C	F	N	P
NR-bare	5.00	6.51								
NR-H	4.96	6.37	0.92	1.22						
NR-H-O	4.60	6.37	0.89		6.73					
NR-H-S	4.87	6.36	0.90			6.49				
NR-H-C	5.03	6.34	0.91				4.45			
NR-H-F	4.76	6.35	0.90					7.58		
NR-H-2F	4.50	6.25	0.90					7.57		
NR-H-N	4.66	6.41	0.85						5.74	
NR-H-P	5.08	6.40	0.90							5.27

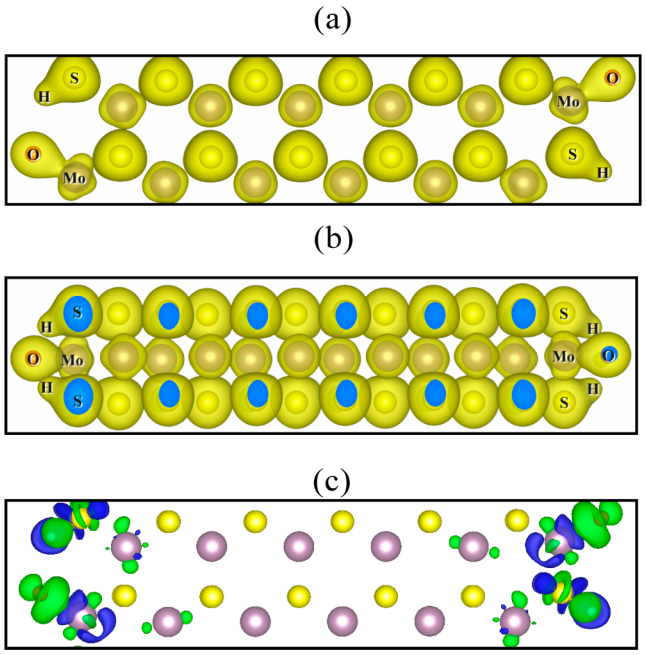

Figure 5. Charge density distribution for A12MoS$_2$NR-H-O for (a) top view and (b) side view. Yellow: charge density isosurface 0.09 e/Å^{-3}. (c) Charge density difference (calculated by the charge density of A12MoS$_2$NR-H-O minus the charge densities of A12MoS$_2$NR and isolated H and isolated O at their corresponding positions). Green: accumulation of electron. Blue: loss of electron.

(33% of total DOS). For the CBM of A12MoS$_2$NR-H, the d_{xy}, d_{z^2}, and $d_{x^2-y^2}$ orbitals of the edge Mo atom play a major role (about 57% of total DOS). The d_{z^2} and $d_{x^2-y^2}$ orbitals of the Mo atom next to the edge atom offer 9% of total DOS, and the remaining Mo atoms, 12%. Seventeen percent of total DOS comes from the S atoms and only 5% DOS comes from the H atoms. The contribution of the H atom itself to DOS is minimal. An obvious change is that several bands in the vicinity of the energy 1.0 eV above the conduction band bottom in A12MoS$_2$NR-bare (compare Figure 3a,b) disappear due to H termination.

The VBM of A12MoS$_2$NR-bare is attributed to the d_{xy}, d_{z^2}, and $d_{x^2-y^2}$ orbitals of the edge Mo atoms (about 29% of total DOS), the Mo atoms next to the edge (about 7%), the other inner Mo atoms (about 38%), and all S atoms (about 26%). The compositions of VBM DOS of A12MoS$_2$NR-H originate in the d_{z^2} and $d_{x^2-y^2}$ orbitals of edge Mo atoms (about 23% of total DOS), the Mo atoms next to the edge (about 30%), the other inner Mo atoms (about 24%), and the S atoms (about 21%). The H atoms only contribute about 2%.

To sum up, the edge Mo atoms contribute most to the frontier orbitals of MoS$_2$ ribbons and no significant DOS variations happen for PDOS of the edge Mo atoms in A12MoS$_2$NR-bare and A12MoS$_2$NR-H. Although the H termination makes A12MoS$_2$NR-H more stable, its influence on the band gap is minimal.

c. H and O (S) Hybrid Edge-Terminated AMoS$_2$NR. Inspired by results on H, B, C, N, O, and F absorbed MoS$_2$ infinite monolayers,[55] we carry out a first-principles study of the electronic properties of non-metal atom functionalized armchair MoS$_2$ nanoribbons. We find that hybrid edge functionalization is an effective way to engineer the band gap of AMoS$_2$NRs (Figure 3c,d).

We introduce hybrid edge functionalization by O on edge Mo atoms and H on edge S atoms, respectively (see Figure 1b for AMoS$_2$NR-H-O). As previously mentioned, Figure 2b gives the energy band gap as a function of the ribbon width from N_a = 8 to N_a = 20 for AMoS$_2$NR-H-O. With the increase of N_a, the band gap of AMoS$_2$NR-H-O approaches 1.43 eV, which is larger than that of the bulk MoS$_2$ system (about 0.86 eV) and is close to that of the monolayer MoS$_2$ (about 1.67 eV). More importantly, this band gap is close to the visible light range precisely needed by the solar cells. Such hybrid edge termination may open up new application possibilities for photoelectronic devices in the future. In addition, from Table 1, one may find that the binding energy of A12MoS$_2$NR-H-O is −5.81 eV. Therefore, A12MoS$_2$NR-H-O is more stable than A12MoS$_2$NR-H. The binding energy of A12MoS$_2$NR-H-X with X = S, F, C, N, P is also smaller than that of A12MoS$_2$NR-H. So our non-metal hybrid passivation enhances the stability of armchair MoS$_2$ ribbons.

To understand the reason for the changes in the band structure, we analyze both the projected density of states (PDOS) and the charge transfer of A12MoS$_2$NR-H-O. In Figure 4c, total DOS and PDOS of A12MoS$_2$NR-H-O are given. For CBM, d_{xy}, d_{z^2}, and $d_{x^2-y^2}$ orbitals of the very and the next edge Mo atoms almost account for 36% and 32% of the total DOS, the other Mo atoms offer only 2%. The rest are contributed by the S atoms (about 20%), O atoms (about 8%), and H atoms (about 2% of total DOS). For VBM, d_{xy}, d_{z^2}, and $d_{x^2-y^2}$ orbitals of the edge Mo only offer 6% of the total DOS, and the next edge Mo atoms offer about 13%. The contribution of other Mo atoms increases to about 53%. The rest of the contribution mainly comes from S atoms (about 28%), and the contribution from O atoms and H atoms is negligible. So we can conclude that due to the appearance of O atoms, the PDOS of edge Mo atoms drops dramatically in both VBM and CBM in A12MoS$_2$NR-H-O. This causes the obvious shifts of CBM and VBM in A12MoS$_2$NR-H-O and fortunately leads to the dramatic increase of the energy band gap.

DOI: 10.1021/acs.jpcc.5b04747
J. Phys. Chem. C XXXX, XXX, XXX−XXX

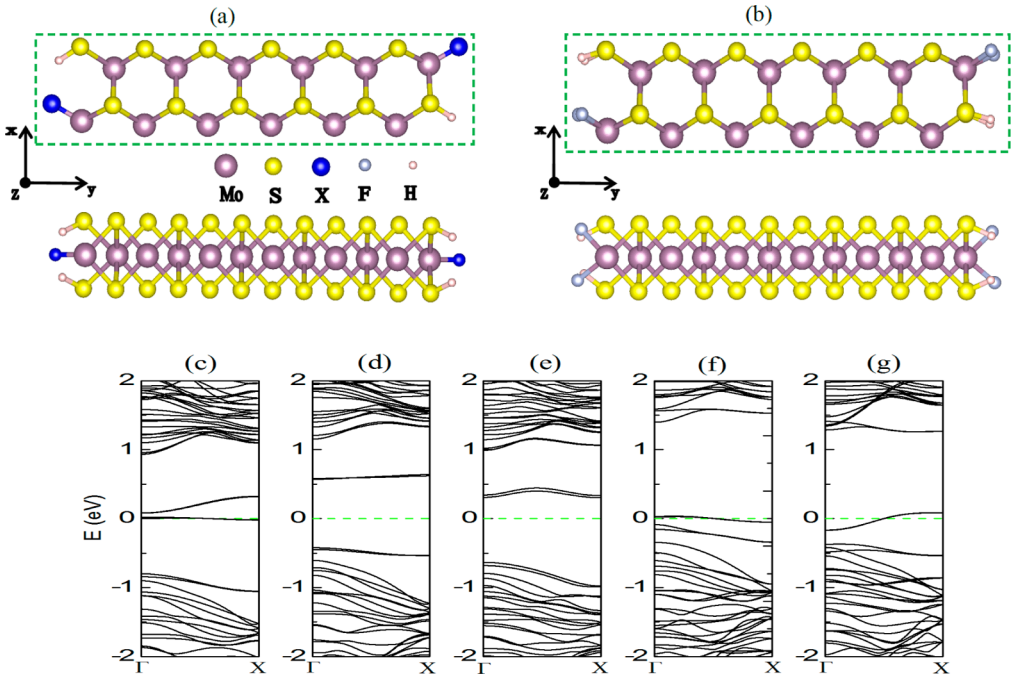

Figure 6. Top and side views of structures for (a) A12MoS_2NR-H-X (X = F, C, N, P) and (b) A12MoS_2NR-H-2F. Energy band structures for (c) A12MoS_2NR-H-F, (d) A12MoS_2NR-H-2F, (e) A12MoS_2NR-H-C, (f) A12MoS_2NR-H-N, and (g) A12MoS_2NR-H-P.

We also quantitatively analyze the charge transfer with the help of Bader charge analysis.[56] Table 2 lists the charges on the edge atoms of different A12MoS_2NRs. In A12MoS_2NR-H, each H atom bonding with edge S atom has the charge 0.92*e* (here, 1*e* = 1.6×10^{-19} C). However, the H atom near the edge Mo atom has a charge of 1.22*e* and shows high electronegativity. Finally, the charges on the S atom changes 0.14*e*, but no evident charge difference appears at edge Mo atom whose orbitals are mainly responsible for the frontier orbitals of the energy band gap. In A12MoS_2NR-H-O, charges have a remarkable redistribution. Each O atom has the highest charge value of 6.73*e*, causing obvious reduction of the charge on the edge Mo atom (0.4*e* smaller than that in the structure A12MoS_2NR-bare). The Bader charge analysis supports the conclusion that the edge Mo and the hybrid O form a new σ-bond, leading to the charge redistribution of edge Mo and increases the band gap energy.

Naturally, we consider H and S hybrid edge termination because O and S are all together in the same group on the periodic table. The band structure of A12MoS_2NR-H-S is shown in Figure 3d. S and H edge-terminated armchair nanoribbons do have the large indirect band gap around 1.09 eV, much larger than the band gap of AMoS_2NR-bare (Table 1). Analysis of the PDOS of A12MoS_2NR-H-S shows the composition of frontier orbitals is different from that of A12MoS_2NR-H-O (Figure 4c,d). From Table 2 we can find each external S atom has a charge value of 6.49*e* that is higher than the charge on the edge S atom (6.36*e*). The external S atom also gives rise to the reduction of charge value on corresponding edge Mo atom. Although the charge on the edge Mo is 0.13*e* smaller than that in the structure A12MoS_2NR-bare, it is still 0.27*e* larger than that in A12MoS_2NR-H-O. This is related to the relative electronegativity of the external S atom and O atom.

Furthermore, one can image that the electron clouds originating from the orbitals of edge Mo and O tend to overlap with each other. The overlapped electron clouds will form the new bonds. Panels a and b of Figure 5 show the charge density distribution of A12MoS_2NR-H-O. Each O atom has two sp hybrid orbitals along the line direction of Mo and O. One sp hybrid orbital points toward Mo atom and forms a σ-bond with Mo. The other sp hybrid orbital becomes a lone pair pointing outward.[57] In addition, the analysis of the charge density difference in Figure 5c shows a charge accumulation on O atoms and charge depletion on corresponding edge Mo atoms, which is consistent with the charge transfer analysis.

d. Other Non-metal Atom Passivated Armchair Nanoribbons. In the above, we get the information about A12MoS_2NR-H-X nanoribbons with X = O and S. Now we explore the electronic structures for A12MoS_2NR-H-X with X = F, C, N, P, 2F, respectively. In Figure 6a,b, we give the top view and side view of the structures for AMoS_2NR-H-X.

Functionalization with one F atom at the edge Mo atom and one H atom at the edge S atom (A12MoS_2NR-H-F) leads to a metallic feature (Figure 6c). Interestingly, another promising F edge-terminated pattern is A12MoS_2NR-H-2F with each edge S atom terminated by one H atom and each edge Mo atom terminated by two F atoms, which gives rise to a direct band gap of 0.99 eV, as shown in Figure 6d. Table 2 shows that edge Mo atom in A12MoS_2NR-H-F and A12MoS_2NR-H-2F are 4.76*e* and 4.5*e*, respectively. Clearly, different terminated F and H hybrid passivation patterns will give rise to different charge distributions of edge Mo atoms, which induce different electronic properties. Then, A12MoS_2NR-H-C is found to be a direct semiconductor with a band gap of 0.94 eV (Figure 6e). Compared to the charge distribution on pristine MoS_2 nanoribbon, the value of charge on the edge Mo atom of A12MoS_2NR-H-C is 5.03*e* (has almost no change with that of A12MoS_2NR-bare). In fact, this hybrid passivation will make a different orbital interaction between the saturated C atom and the corresponding Mo atom. Finally, we calculate N and P edge-terminated situations (A12MoS_2NR-H-N and A12MoS_2NR-H-P); metallic features are found in both (Figure 6f,g). The charge on the edge Mo atom of A12MoS_2NR-H-N is 4.66*e* smaller than the charge on A12MoS_2NR-H-P

DOI: 10.1021/acs.jpcc.5b04747
J. Phys. Chem. C XXXX, XXX, XXX−XXX

(5.08*e*). Besides, we can find that the charges on the N atom are larger than those on the P atom, which may be ascribed to the larger electronegativity of N. By and large, the charge redistribution of the edge Mo atoms caused by the saturated atoms will change the internal hybridization pattern, which gives rise to new edge states that inevitably induce distinct electronic properties.

IV. CONCLUSIONS

In summary, we have performed a first-principles study of armchair single-layer MoS_2 nanoribbons with various passivations. We show that hybrid passivation can tune the band gap of the nanoribbons. It is found that the hybrid passivation by both H and X (X = O, S, F, C, N, P) can dramatically reshape the electronic properties. In particular, $AMoS_2$NR-H-O, $AMoS_2$NR-H-S, and $AMoS_2$NR-H-C achieve the remarkable band gaps of 1.43, 1.09, and 0.94 eV, respectively. $AMoS_2$NR-H-F, $AMoS_2$NR-H-N, and $AMoS_2$NR-H-P exhibit metallic features. If each edge S atom is saturated by one H atom and each edge Mo is saturated by two F atoms in the A12MoS_2NR-H-2F system, a direct band gap of 0.99 eV is obtained. Our results suggest the potential application of armchair single-layer MoS_2 nanoribbon in novel nanoelectronics and photovoltaic devices.

AUTHOR INFORMATION

Corresponding Authors

*E-mail: wanlh@szu.edu.cn. Tel: +86-755-26535355.
*E-mail: ywei@szu.edu.cn. Tel: +86-755-26530589.

Notes

The authors declare no competing financial interest.

ACKNOWLEDGMENTS

We gratefully acknowledge the support from National Natural Science Foundation of China with Grant Nos. 11374246, 11304205, and 11447159. Y. Zhao acknowledges the support from the Singapore National Research Foundation through the Competitive Research Programme under Project No. NRF-CRP5-2009-04.

REFERENCES

(1) Wang, Q.; Kalantar-Zadeh, K.; Kis, A.; Coleman, J. N.; Strano, M. S. Electronics and Optoelectronics of Two-dimensional Transition Metal Dichalcogenides. *Nat. Nanotechnol.* **2012**, *7*, 699−712.

(2) Splendiani, A.; Sun, L.; Zhang, Y.; Li, T.; Kim, J.; Chim, C. Y.; Galli, G.; Wang, F. Emerging Photoluminescence in Monolayer MoS_2. *Nano Lett.* **2010**, *10*, 1271−1275.

(3) Cai, J.; Ruffieux, P.; Jaafar, R.; Bieri, M.; Braun, T.; Blangkenburg, S.; Muoth, M.; Seitsonen, A. P.; Saleh, M.; Feng, X.; et al. Atomically Precise Bottom-up Fabrication of Graphene Nanoribbons. *Nature* **2010**, *466*, 470−473.

(4) Ohta, T.; Bostwick, A.; Seyller, T.; Horn, K.; Rotenberg, E. Controlling the Electronic Structure of Bilayer Graphene. *Science* **2006**, *313*, 951−954.

(5) Oostinga, J. B.; Heersche, H. B.; Liu, X. L.; Morpurgo, A. F.; Vandersypen, L. M. K. Gate-induced Insulating State in Bilayer Graphene Devices. *Nat. Mater.* **2008**, *7*, 151−157.

(6) Dong, X.; Shi, Y.; Zhao, Y.; Chen, D. M.; Ye, J.; Yao, Y. G.; Gao, F.; Ni, Z.; Yu, T.; Shen, Z. X.; et al. Symmetry Breaking of Graphene Monolayers by Molecular Decoration. *Phys. Rev. Lett.* **2009**, *102*, 135501.

(7) Chen, D. M.; Shenai, P. M.; Zhao, Y. Tight Binding Description on the Band Gap Opening of Pyrene-dispersed Graphene. *Phys. Chem. Chem. Phys.* **2011**, *13*, 1515−1520.

(8) Novoselov, K. S.; Fal, V. I.; Colombo, L.; Gellert, P. R.; Schwab, M. G.; Kim, K. A Roadmap for Graphene. *Nature* **2012**, *490*, 192−200.

(9) Elias, D. C.; Nair, R. R.; Mohiuddin, T. M. G.; Morozov, S. V.; Blake, P.; Halsall, M. P.; Ferrari, A. C.; Boukhvalov, D. W.; Katsnelson, M. I.; Geim, A. K.; et al. Control of Graphene's Properties by Reversible Hydrogenation: Evidence for Graphane. *Science* **2009**, *323*, 610−613.

(10) Kim, K.; Choi, J. Y.; Kim, T.; Cho, S. H.; Chung, H. J. A Role for Graphene in Silicon Based Semiconductor Devices. *Nature* **2011**, *479*, 338−344.

(11) Shih, C. J.; Wang, Q. H.; Jin, Z.; Paulus, G.; Blankschtein, D.; Jarillo-Htrrero, P.; Strano, M. Disorder Imposed Limits of Mono-and Bilayer Graphene Electronic Modification Using Covalent Chemistry. *Nano Lett.* **2013**, *13*, 809−817.

(12) Das, S.; Chen, H. Y.; Penumatcha, A. V.; Appenzeller, J. High Performance Multilayer MoS_2 Transistors with Scandium Contacts. *Nano Lett.* **2013**, *13*, 100−105.

(13) Zhang, W.; Chuu, C. P.; Huang, J. K.; Chen, C. H.; Tsai, M. L.; Chang, Y. H.; Liang, C. T.; Chen, Y. Z.; Chueh, Y. L.; He, J. H.; et al. Ultrahigh-gain Photodetectors Based on Atomically Thin Graphene-MoS_2 Heterostructures. *Sci. Rep.* **2014**, *4*, 3826.

(14) Bernardi, M.; Palummo, M.; Grossman, J. C. Extraordinary Sunlight Absorption and One Nanometer Thick Photovoltaics Using Two-dimensional Monolayer Materials. *Nano Lett.* **2013**, *13*, 3664−3670.

(15) Musso, T.; Kumar, P. V.; Foster, A. S.; Grossman, J. Graphene Oxide as a Promising Hole Injection Layer for MoS_2-Based Electronic Devices. *ACS Nano* **2014**, *8*, 11432−11439.

(16) Radisavljevic, B.; Kis, A. Mobility Engineering and a Metal−insulator Transition in Monolayer MoS_2. *Nat. Mater.* **2013**, *12*, 815−820.

(17) Zeng, H.; Dai, J.; Yao, W.; Xiao, D.; Cui, X. Valley Polarization in MoS_2 Monolayers by Optical Pumping. *Nat. Nanotechnol.* **2012**, *7*, 490−493.

(18) Shih, C. J.; Wang, Q. H.; Son, Y.; Jin, Z.; Blankschtein, D.; Strano, M. S. Tuning On−off Current Ratio and Field-Effect Mobility in a MoS_2−Graphene Heterostructure via Schottky Barrier Modulation. *ACS Nano* **2014**, *8*, 5790−5798.

(19) Mak, K. F.; Lee, C.; Hone, J.; Shan, J.; Heinz, T. F. Atomically Thin MoS_2: A New Direct-gap Semiconductor. *Phys. Rev. Lett.* **2010**, *105*, 136805.

(20) Han, S. W.; Kwon, H.; Kim, S.; Ryu, S.; Yun, W.; Kim; Seong, K.; Hwang, J.; Kang, J.; Baik, J.; Shin, H.; Hong, H. Band-gap Transition Induced by Interlayer Van der Waals Interaction in MoS_2. *Phys. Rev. B: Condens. Matter Mater. Phys.* **2011**, *84*, 045409.

(21) Verble, J. L.; Wietling, T. J.; Reed, P. R. Rigid-layer Lattice Vibrations and Van der Waals Bonding in Hexagonal MoS_2. *Solid State Commun.* **1972**, *11*, 941−944.

(22) Shi, Y.; Zhou, W.; Lu, A. Y.; Fang, W.; Lee, Y. H.; Hsu, A. L.; Kim, S. M.; Kim, K. K.; Yang, H. Y.; Li, L. J.; et al. Van der Waals Epitaxy of MoS_2 Layers Using Graphene as Growth Templates. *Nano Lett.* **2012**, *12*, 2784−2791.

(23) Coleman, J. N.; Lotya, M.; Oneill, A.; Bergin, S.; King, P.; Khan, U.; Young, K.; Gaucher, A.; De, S.; Smith, R.; et al. Two-dimensional Nanosheets Produced by Liquid Exfoliation of Layered Materials. *Science* **2011**, *331*, 568−571.

(24) Helveg, S.; Lauritsen, J. V.; Lægsgaard, E.; Stensgaard, I.; Nørskov, J. K.; Clausen, B. S.; Topsøe, H.; Besenbacher, F. Atomic-scale Structure of Single-layer MoS_2 Nanoclusters. *Phys. Rev. Lett.* **2000**, *84*, 951−954.

(25) Liu, K. K.; Zhang, W.; Lee, Y. H.; Lin, Y. C.; Chang, M. T.; Su, C. Y.; Chang, C. S.; Li, H.; Shi, Y.; Zhang, H.; et al. Growth of Large-area and Highly Crystalline MoS_2 Thin Layers on Insulating Substrates. *Nano Lett.* **2012**, *12*, 1538−1544.

(26) Lee, Y. H.; Yu, L.; Wang, H.; Fang, W.; Ling, X.; Shi, Y.; Lin, C. T.; Huang, J. K.; Chang, M. T.; Chang, C. S.; et al. Synthesis and Transfer of Single-layer Transition Metal Disulfides on Diverse Surfaces. *Nano Lett.* **2013**, *13*, 1852−1857.

(27) Xia, Y.; Yang, P.; Sun, Y.; Wu, Y.; Mayers, B.; Gates, B.; Yin, Y.; Kim, F.; Yan, H. One-dimensional Nanostructures: Synthesis, Characterization, and Applications. *Adv. Mater.* **2003**, *15*, 353−389.

DOI: 10.1021/acs.jpcc.5b04747
J. Phys. Chem. C XXXX, XXX, XXX−XXX

(28) Dolui, K.; Pemmaraju, C. D.; Sanvito, S. Electric Field Effects on Armchair MoS_2 Nanoribbons. *ACS Nano* **2012**, *6*, 4823−4834.
(29) Guo, H.; Lu, N.; Wang, L.; Wu, X.; Zeng, X. C. Phosphorene Nanoribbons, Phosphorus Nanotubes, and Van der Waals Multilayers. *J. Phys. Chem. C* **2014**, *118*, 14051.
(30) Yang, S.; Li, D.; Zhang, T.; Tao, Z.; Chen, J. First-principles Study of Zigzag MoS_2 Nanoribbon as a Promising Cathode Material for Rechargeable Mg Batteries. *J. Phys. Chem. C* **2012**, *116*, 1307−1312.
(31) Wang, Z.; Li, H.; Liu, Z.; Shi, Z.; Lu, J.; Suenaga, K.; Joung, S. K.; Okazaki, T.; Gu, Z.; Zhou, J.; et al. Mixed Low-dimensional Nanomaterial: 2D Ultranarrow MoS_2 Inorganic Nanoribbons Encapsulated in Quasi-1D Carbon Nanotubes. *J. Am. Chem. Soc.* **2010**, *132*, 13840−13847.
(32) Liu, X.; Xu, T.; Wu, X.; Zhang, Z.; Yu, J.; Qiu, H.; Hong, J. H.; Jin, C. H.; Li, J. X.; Wang, X. R.; et al. Top−down Fabrication of Sub-nanometre Semiconducting Nanoribbons Derived from Molybdenum Disulfide Sheets. *Nat. Commun.* **2013**, *4*, 1776.
(33) Cai, Y.; Zhang, G.; Zhang, Y. W. Polarity-reversed Robust Carrier Mobility in Monolayer MoS_2 Nanoribbons. *J. Am. Chem. Soc.* **2014**, *136*, 6269−6275.
(34) Pan, H.; Zhang, Y. W. Edge-dependent Structural, Electronic and Magnetic Properties of MoS_2 Nanoribbons. *J. Mater. Chem.* **2012**, *22*, 7280−7290.
(35) Cai, Y.; Bai, Z.; Pan, H.; Feng, Y. P.; Yakobson, B.; Zhang, Y. W. Constructing Metallic Nanoroads on a MoS_2 Monolayer via Hydrogenation. *Nanoscale* **2014**, *6*, 1691−1697.
(36) Botello-Méndez, A. R.; Lopez-Urias, F.; Terrones, M.; Terrones, H. Metallic and Ferromagnetic Edges in Molybdenum Disulfide Nanoribbons. *Nanotechnology* **2009**, *20*, 325703.
(37) Ouyang, F. P.; Yang, Z. X.; Ni, X.; Wu, N. N.; Chen, Y. Hydrogenation-Induced Edge Magnetization in Armchair MoS_2 Nanoribbon and Electric Field Effects. *Appl. Phys. Lett.* **2014**, *104*, 071901.
(38) Tian, X.; Liu, L.; Du, Y.; Gu, J.; Xu, J. B.; Yakobson, B. Effects of 3d Transition-metal Doping on Electronic and Magnetic Properties of MoS_2 Nanoribbons. *Phys. Chem. Chem. Phys.* **2015**, *17*, 1831−1836.
(39) Li, W.; Guo, M.; Zhang, G.; Zhang, Y. W. Edge-Specific Au/Ag Functionalization-Induced Conductive Paths in Armchair MoS_2 Nanoribbons. *Chem. Mater.* **2014**, *26*, 5625−5631.
(40) Liu, H.; Gu, J.; Ye, P. D. Nanoribbon Transistors: Transition From Depletion Mode to Enhancement Mode by Channel-Width Trimming. *IEEE Electron Device Lett.* **2012**, *33*, 1273−1275.
(41) Ghosh, R. K.; Mahapatra, S. Direct Band-to-Band Tunneling in Reverse Biased Nanoribbon pn Junctions. *IEEE Trans. Electron Devices* **2013**, *60*, 274.
(42) Li, Y.; Zhou, Z.; Zhang, S.; Chen, Z. MoS_2 Nanoribbons: High Stability and Unusual Electronic and Magnetic Properties. *J. Am. Chem. Soc.* **2008**, *130*, 16739−16744.
(43) Radisavljevic, B.; Radenovic, A.; Brivio, J.; Giacometti, V.; Kis, A. Single-layer MoS_2 Transistors. *Nat. Nanotechnol.* **2011**, *6*, 147.
(44) Kou, L. Z.; Tang, C.; Zhang, Y.; Heine, T.; Chen, C. F.; Frauenheim, T. Tuning Magnetism and Electronic Phase Transitions by Strain and Electric Field in Zigzag MoS_2 Nanoribbons. *J. Phys. Chem. Lett.* **2012**, *3*, 2934.
(45) Sagynbaeva, M.; Panigrahi, P.; Yunguo, L.; Ramzan, M.; Ahuja, R. Tweaking the Magnetism of MoS_2 Nanoribbon with Hydrogen and Carbon Passivation. *Nanotechnology* **2014**, *25*, 165703.
(46) Li, X. S.; Xin, Q.; Guo, X. X.; Grange, P.; Delmon, B. Reversible Hydrogen Adsorption on MoS_2 Studied by Temperature-programmed Desorption and Temperature-programmed Reduction. *J. Catal.* **1992**, *137*, 385−393.
(47) Kresse, G.; Furthmuller, J. Efficiency of Ab-initio Total Energy Calculations for Metals and Semiconductors Using a Plane-wave Basis Set. *Comput. Mater. Sci.* **1996**, *6*, 15−50.
(48) Kresse, G.; Furthmuller, J. Efficient Iterative Schemes for Ab Initio Total-energy Calculations Using a Plane-wave Basis Set. *Phys. Rev. B: Condens. Matter Mater. Phys.* **1996**, *54*, 11169−11186.
(49) Perdew, J. P.; Burke, K.; Ernzerhof, M. Generalized Gradient Approximation Made Simple. *Phys. Rev. Lett.* **1996**, *77*, 3865.
(50) Perdew, J. P.; Chevary, J. A.; Vosko, S. H.; Jackson, K. A.; Pederson, M. R.; Singh, D. J.; Fiolhais, C. Applications of the Generalized Gradient Approximation for Exchange and Correlation. *Phys. Rev. B: Condens. Matter Mater. Phys.* **1992**, *46*, 6671−6687.
(51) Waldron, D.; Haney, P.; Larade, B.; MacDonald, A.; Guo, H. Nonlinear Spin Current and Magneto Resistance of Molecular Tunnel Junctions. *Phys. Rev. Lett.* **2006**, *96*, 166804.
(52) Wang, B.; Wang, J.; Guo, H. Ab Initio Calculation of Transverse Spin Current in Graphene Nanostructures. *Phys. Rev. B: Condens. Matter Mater. Phys.* **2009**, *79*, 165417.
(53) Bollinger, M.; Lauritsen, J.; Jacobsen, K.; Norskov, J.; Helveg, S.; Besenbacher, F. One-dimensional Metallic Edge States in MoS_2. *Phys. Rev. Lett.* **2001**, *87*, 196803.
(54) In our calculation, we do not consider the spin polarization because the armchair ribbon of MoS_2 has no magnetic effect at the edge sites for our hybrid passivation.
(55) He, J.; Wu, K.; Sa, R.; Li, Q.; Wei, Y. Magnetic Properties of Nonmetal Atoms Absorbed MoS_2 Monolayers. *Appl. Phys. Lett.* **2010**, *96*, 082504.
(56) Henkelman, G.; Arnaldsson, A.; Jonsson, H. A Fast and Robust Algorithm for Bader Decomposition of Charge Density. *Comput. Mater. Sci.* **2006**, *36*, 354−360.
(57) Lopez-Bezanilla, A.; Huang, J. S.; Terrones, H.; Sumpter, B. G. Boron Nitride Nanoribbons Become Metallic. *Nano Lett.* **2011**, *11*, 3267−3273.

DOI: 10.1021/acs.jpcc.5b04747
J. Phys. Chem. C XXXX, XXX, XXX−XXX